JBC RESEARCH ARTICLE

The evolutionary divergence of receptor guanylyl cyclase C has implications for preclinical models for receptor-directed therapeutics

Received for publication, October 23, 2023, and in revised form, November 16, 2023 Published, Papers in Press, November 27, 2023,
https://doi.org/10.1016/j.jbc.2023.105505

Vishwas Mishra[1], **Kritica Sharma**[1], **Avipsa Bose**[1], **Pierre Maisonneuve**[2], **and Sandhya S. Visweswariah**[1,*]

From the [1]*Department of Developmental Biology and Genetics, Indian Institute of Science, Bengaluru, India;* [2]*UMR 5248 - Chemistry & Biology of Membranes and Nano-Objects, CNRS - Université de Bordeaux, Institut Européen de Chimie et Biologie, Pessac, France*

Reviewed by members of the JBC Editorial Board. Edited by Joseph Jez

Mutations in receptor guanylyl cyclase C (GC-C) cause severe gastrointestinal disease, including meconium ileus, early onset acute diarrhea, and pediatric inflammatory bowel disease that continues into adulthood. Agonists of GC-C are US Food and Drug Administration-approved drugs for the treatment of constipation and irritable bowel syndrome. Therapeutic strategies targeting GC-C are tested in preclinical mouse models, assuming that murine GC-C mimics human GC-C in its biochemical properties and downstream signaling events. Here, we reveal important differences in ligand-binding affinity and GC activity between mouse GC-C and human GC-C. We generated a series of chimeric constructs of various domains of human and mouse GC-C to show that the extracellular domain of mouse GC-C contributed to log-orders lower affinity of mouse GC-C for ligands than human GC-C. Further, the Vmax of the murine GC domain was lower than that of human GC-C, and allosteric regulation of the receptor by ATP binding to the intracellular kinase-homology domain also differed. These altered properties are reflected in the high concentrations of ligands required to elicit signaling responses in the mouse gut in preclinical models and the specificity of a GC inhibitor towards human GC-C. Therefore, our studies identify considerations in using the murine model to test molecules for therapeutic purposes that work as either agonists or antagonists of GC-C, and vaccines for the bacterial heat-stable enterotoxin that causes watery diarrhea in humans.

Gastrointestinal function is integral to the well-being of an organism, and alterations in intestinal epithelial cell function and the microbiome have important physiological outcomes (1). For example, diarrheal disease is mediated by the action of toxins produced by pathogenic strains of *Escherichia coli*, and prolonged or frequent episodes of diarrheal disease can result in stunting of growth and intellectual disabilities (1, 2). Efforts to identify therapeutic strategies to combat common forms of diarrheal disease utilize mice as models for testing drugs or inhibitors of signaling pathways that result in diarrhea (3, 4). However, commonly used strains of mice, such as C57BL/6, do not demonstrate excessive watery stools or stool passage frequency as seen in humans (5, 6). This has been attributed to an evolutionary adaptation of the gut to the environment and diet of rodents in comparison to humans. Therefore, understanding the molecular basis underlying divergent gut responses in rodents and humans would further our ability to interpret results from preclinical trials in mouse models.

Guanylyl cyclase C (GC-C) is the receptor for heat-stable enterotoxin (ST) produced by pathogenic strains of *E. coli* such as enterotoxigenic *E. coli* (ETEC), the causative agent of enterotoxigenic *E. coli*–mediated diarrhea in children and traveler's diarrhea (1, 7). GC-C is predominantly expressed on the apical surface of intestinal epithelial cells and serves as the receptor for the endogenous peptide ligands, guanylin and uroguanylin. This single-pass membrane receptor possesses a ligand-binding extracellular domain (ECD), a transmembrane region, a juxta-membrane domain, an allosteric regulator pseudokinase or kinase homology domain (KHD), a short linker region, a catalytic guanylyl cyclase domain (GCD), and a C-terminal tail or domain (8, 9). Activation of GC-C by ligands increases intracellular 3′,5′-cyclic GMP (cGMP) levels, which in turn can modulate ion channels and thus regulate salt and water homeostasis in the intestine. Dysregulation of the GC-C signaling due to human mutations results in chronic gastrointestinal disease (9). Activating mutations result in congenital secretory diarrhea that manifests as inflammatory bowel disease at later stages of life. Loss-of-function mutations result in meconium ileus, which is the inability of the newborn to pass the first stool (9). Therefore, GC-C is critical for regulating fluid-ion homeostasis in the gut.

Mice have been used as a preclinical model for developing the US Food and Drug Administration-approved GC-C agonists linaclotide and plecanatide (4, 10). These peptides are considered one of the most potent drugs to alleviate symptoms of constipation-predominant irritable bowel syndrome and also relieve patients from visceral pain (7, 11). GC-C KO mice have been used to understand the intestinal and extraintestinal roles of GC-C (12–14). Recently, we reported a mouse model with a hyperactive mutation in GC-C, which mimics Familial

* For correspondence: Sandhya S. Visweswariah, sandhya@iisc.ac.in.

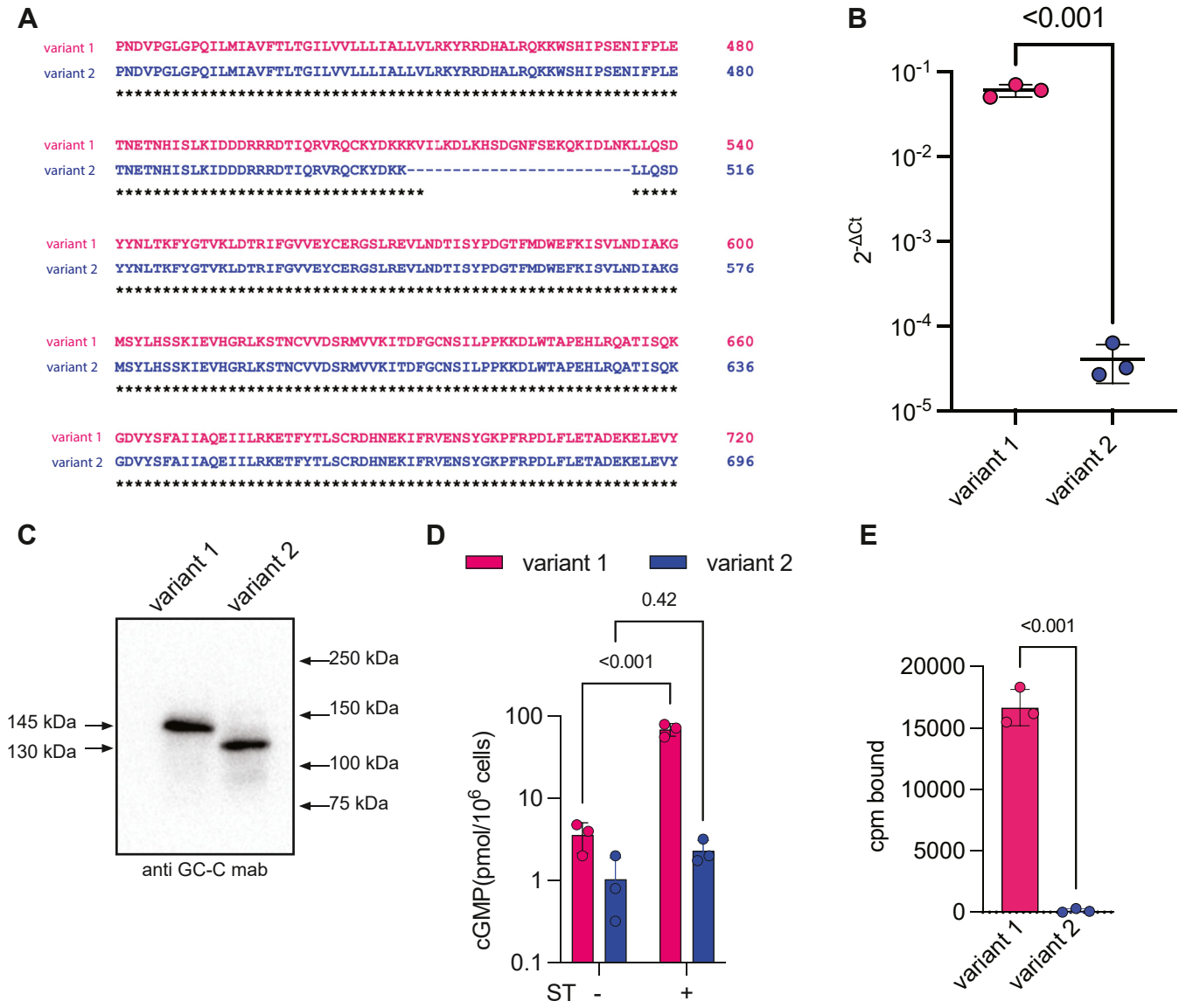

Figure 1. Characterization of splice variant of mouse *Gucy2c*. *A*, sequence alignment of the KHDs of variant 1 and variant 2 of mouse *Gucy2c*, indicating the deletion of amino acids encoded in exon 14 of variant 1 that is absent in variant 2. *B*, transcript levels of mouse *Gucy2c* variant 1 and variant 2 in the ileum of C57BL/6 mouse determined by quantitative reverse transcription polymerase chain reaction and normalized to the expression of *Gapdh*. Each *dot* represents an individual mouse, and values shown are the mean ± SD; *p* values were determined using an unpaired, two-tailed *t* test. *C*, Western blot analysis of lysates prepared from HEK293E cells expressing either mouse GC-C variant 1 or variant 2 using mAb to GC-C. *D*, HEK293E cells expressing either mouse GC-C variant 1 or variant 2 were treated with medium alone or 10^{-6} M ST and cGMP estimated by radioimmunoassay. Values shown are the mean ± SD from three independent experiments performed with duplicate experimental determinations. Data was analyzed using two-way ANOVA with multiple comparisons and *p* values shown. *E*, radiolabeled ST binding to monolayer cultures of HEK293E cells expressing either mouse GC-C variant 1 or variant 2. Values shown are the mean ± SD from three independent experiments with two technical duplicates; *p* values are shown are from an unpaired, two-tailed *t* test. cGMP, 3′,5′-cyclic GMP; GC-C, guanylyl cyclase-C; KHD, kinase homology domain; ST, stable enterotoxin.

GUCY2C diarrhea syndrome (FGDS) and GC-C–mediated diarrhea (6). However, we noted that significantly higher concentrations of GC-C ligands were required to activate the receptor and elicit cGMP production than for human GC-C (hGC-C). Surprisingly, although mouse has been used as a preclinical model to develop GC-C agonists and to study GC-C biology, the biochemical properties of mouse GC-C (mGC-C) have not been studied.

There is some evidence of differences between human and mouse GC-C, such as, mice lacking GC-C are resistant to ST-induced fluid accumulation but display no signs of constipation or defects in intestinal fluid-ion homeostasis even upon oral administration of fluids containing high amounts of salt (12). On the other hand, human patients with inactivating mutations in GC-C display intestinal obstructions and meconium ileus (9, 15). Similarly, GC-C inhibitors developed against hGC-C fail to act on mGC-C (16), and the dose of GC-C agonists used during preclinical trials on mouse models are log orders higher than the dose used for humans (4, 11, 17). Whether GC-C plays different functions in the intestine of mice or whether mGC-C differs from hGC-C in terms of its enzymatic properties, efficacy, and potency for agonists and antagonists, is completely unknown.

Here, we report the biochemical properties of mGC-C, a knowledge of which is a prerequisite to deploying mice for preclinical trials of GC-C agonists or using it as a model to study the effect of new molecules to regulate GC-C activity. Mouse GC-C shows significantly lower binding affinity to ligands and GC activity than hGC-C. Using chimeric constructs, we could delineate domains in the receptor that contribute to these divergent activities, and thus allow a greater appreciation of the sites of action of potential therapeutics directed toward patients harboring pathogenic variants of GC-C.

Results

Isoforms of mGC-C expressed in the gut

There are predicted to be two isoforms of mGC-C (accession numbers NP_01120790.1 and NP_659504.2) (18). Aligning these two proteins reveals that isoform or variant 2 (1048 amino acids) is shorter than the full-length protein (1072 amino acids). The amino acids absent in variant 2 are encoded entirely in exon 14, that is deleted in splice variant 2 (Fig. 1*A*; https://www.ncbi.nlm.nih.gov/genome/gdv/browser/gene/?id=14917), and are contained in the KHD. The KHD in hGC-C plays a critical role in modulating ligand-binding activation (19, 20). If variant 2 is compromised in its catalytic activity because of the loss of these amino acids, but could still bind ligand through the ECD, this truncated protein could serve as a "sink" for both endogenous ligands and administered peptides.

We designed primers that would specifically amplify either variant 1 or 2 (Table S1) and monitored their expression in the small intestine of mice by quantitative reverse transcription polymerase chain reaction. As seen in Figure 1*B*, levels of variant 1 were more than 10,000-fold higher than that of variant 2. We expressed both variants in HEK293E cells and saw altered mobility in the migration of the two variants as predicted from the deletion of 24 amino acids in variant 2 (Fig. 1*C*). We stimulated cells expressing either variant 1 or 2 with the ST peptide and observed a significant increase in cGMP levels in cells expressing variant 1 when treated with ST. However, the cGMP levels in cells expressing variant 2 remained unchanged upon ST treatment (Fig. 1*D*). Further, there was a marked reduction in the ligand binding ability of variant 2 (Fig. 1*E*), which could explain the absence of cGMP production in the presence of ST peptide. Further, variant 2 showed undetectable *in vitro* GC activity (data not shown), indicating that the protein, if expressed in the intestine, would be inactive. Variant 2 therefore may not function in the gut or sequester ligand because of its low expression and apparent overall misfolding. Therefore, we focused on variant 1 for the remaining analysis, representing full-length mGC-C.

Reduced ligand-binding affinity of mGC-C

We generated two HEK 293E cell lines stably expressing either hGC-C or mGC-C, respectively. Western blot analysis revealed that mGC-C migrated slower than hGC-C (Fig. 2*A*). We have reported that hGC-C is heavily glycosylated (21, 22), and therefore asked if differential glycosylation of mGC-C accounted for its slower mobility. Membranes from cell lines were treated with PNGase F to remove complex glycosylation from the mature forms of GC-C. While hGC-C migrated at a size predicted by its amino acid sequence, mGC-C continued to show reduced migration (Fig. 2*B*). We then treated transiently transfected HEK 293E cells with tunicamycin, which prevents initial glycosylation of proteins in the endoplasmic reticulum. Western blot analysis still revealed a significant difference in migration between hGC-C and mGC-C, indicating that the altered mobility was a function of the sequences of the two proteins (Fig. 2*C*). The predicted pI of hGC-C is 6.77 while that of mGC-C is 6.38, and there is no appreciable difference in their predicted molecular weights (123,189 for hGC-C and 123,402 for mGC-C). Therefore, the more acidic nature of mGC-C may prevent SDS from efficiently coating the protein to allow migration based on the molecular size alone (23). Alternatively, differential detergent binding to helical regions could result in anomalous migration of these membrane-associated proteins (24).

Sequence alignment of the ECDs of human and mGC-C revealed significant sequence identity in the ECD of GC-C (70.7% sequence identity; Fig. 2*D*). All residues glycosylated in hGC-C are conserved in mGC-C (Fig. 2*D*). However, an additional putative glycosylation site at N188 could be identified in mGC-C. We mutated this residue to alanine to create the N188A mutant mGC-C. However, this mutation did not show a significant change in mobility, suggesting that this residue in mGC-C may not be appreciably glycosylated (Fig. S1).

In radioligand receptor binding assays, the affinity of the ST peptide for mGC-C was a log order lower than that for hGC-C (Fig. 2*E*). The affinities for uroguanylin peptides were also significantly different, both when human uroguanylin was used in displacement assays with hGC-C and mouse uroguanylin used in assays with mGC-C (left panel, homologous displacement), or the peptides were swapped (*i.e.*, mouse uroguanylin and hGC-C and human uroguanylin and mGC-C, heterologous displacement, right panel) (Fig. 2*F*). This indicated that the reduced affinity of mGC-C was independent of the sequence of the uroguanylin peptides (inset Fig. 2*F*). These findings have important implications for using the mouse as a preclinical model to identify peptides/molecules that bind to hGC-C.

We have shown earlier that folding and glycosylation of hGC-C regulates its trafficking to the cell surface (21). A significant fraction of hGC-C is retained in the endoplasmic reticulum, but both plasma membrane- and endoplasmic reticulum–associated hGC-C could bind ST with comparable affinities (21). We applied radiolabeled ST to monolayer cultures of HEK293E cells expressing either hGC-C or mGC-C and monitored the specific binding of radioligand to intact cells. We saw consistently higher binding to cells expressing mGC-C (Fig. 2*G*, upper panel). We prepared membranes from parallelly transfected cells, and by estimating the receptor binding equivalent to the number of cells used in monolayer binding experiments, we determined that the fraction of mGC-C that trafficked to the surface of cells was higher than hGC-C (Fig. 2*G*, lower panel). Therefore, the properties of mGC-C, such as better intracellular folding and interaction with

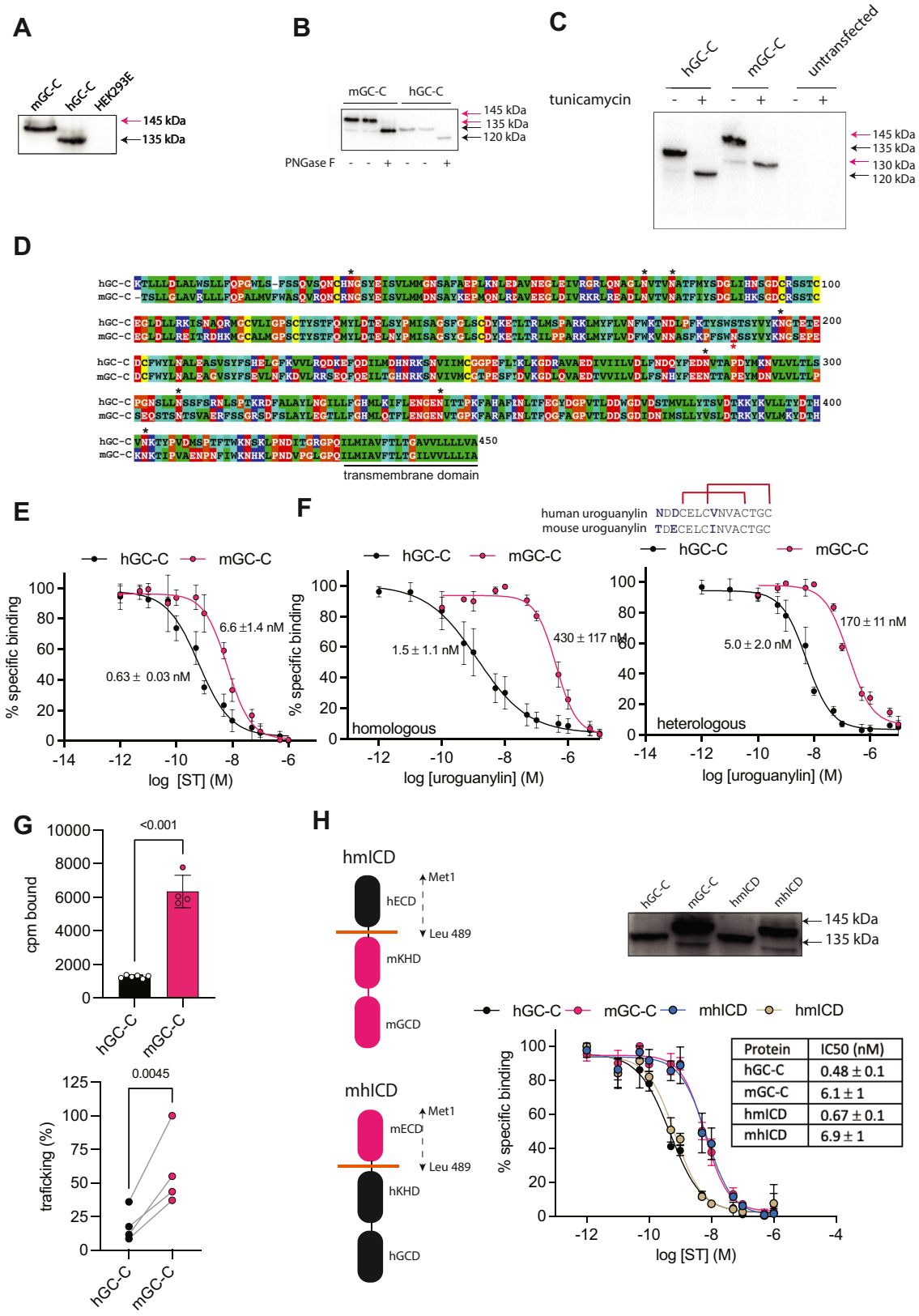

Figure 2. Comparison of the extracellular domains of mouse and human GC-C. *A*, Western blot analysis of membrane protein prepared from HEK293E cells expressing either mouse or human GC-C. Experiments are representative of data from three independent experiments. *B*, Western blot analysis of membrane protein prepared from HEK293E cells expressing either mouse or human GC-C post PNGase F treatment. The blot shown represents an experiment repeated twice from independent membrane preparation. *C*, Western blot of membranes prepared from transfected HEK293E cells treated with tunicamycin. Data is representative of experiments repeated twice. *D*, sequence alignment of the extracellular domain (ECD) of mouse and human GC-C. Highlighted with * are potential N-glycosylation sites in mouse and human GC-C. A *red* * identifies the N188 residue, a potential site for glycosylation in mGC-C. *E*, binding of ^{125}I-labeled ST_{Y72F} peptide to membranes prepared from cells expressing the indicated constructs in the presence of varying

chaperone machinery (21) may allow it to migrate to the plasma membrane more efficiently than hGC-C.

We then asked if the lower binding affinity of mGC-C to its ligands was solely dependent on the ECD. Because of the significant sequence similarity between hGC-C and mGC-C, we constructed chimeric proteins, where the ECDs of the two proteins were swapped (Figs. 2*H* and S2). WT and chimeric proteins were expressed in HEK293E cells. Western blot analysis revealed that the migration of the full-length receptors on SDS gels depended on the ECD, with mGC-C and mhICD chimera migrating slower than the human counterparts (Fig. 2*I*, upper panel). Further, the reduced affinity to the ST peptide was seen with the mhICD chimera, reiterating that distinct biochemical properties were linked to the ECD domains of human and mGC-C (Fig. 2*I*, lower panel).

Reduced GC activity of mGC-C

So far, we have shown that mGC-C has a reduced affinity for its ligands, suggesting that higher concentrations of ligand would be required for maximal stimulation of the receptor. We added ST to cells expressing either hGC-C or mGC-C at a concentration (10^{-6}M) that would saturate both receptors. We observed that intracellular cGMP accumulation in cells expressing mGC-C was ∼10-fold lower than in hGC-C when normalized to the receptor levels on the cell surface (Fig. 3*A*). The dose-response curve with the ST peptide reflected the lower affinity of mGC-C for the ST peptide, resulting in lower efficacy (Fig. 3*B*) with an EC_{50} of ∼50 nM for the peptide applied to cells expressing hGC-C and an EC_{50} of ∼200 nM for cells expressing mGC-C (*p* value 0.01). Further, accumulation of cGMP in cells expressing mGC-C at saturating concentrations of ST (10^{-5} M) was much reduced in comparison with cells expressing hGC-C (Fig. 3*B*). The Vmax for GC activity of mGC-C was >10-fold lower than hGC-C when assays were performed with MnGTP as substrate (Fig. 3*C*; hGC-C, Vmax 8.1 ± 1.7 nmol/pmol receptor; mGC-C 0.3 ± 0.12 nmol/pmol receptor; *p*-value < 0.01). Both receptors showed similar Hill coefficients greater than 1 (hGC-C 1.3 ± 0.4; mGC-C 1.4 ± 0.1), indicating allosteric kinetics, and the K′ for MnGTP was not significantly different (hGC-C, 0.46 ± 0.24 mM; mGC-C, 0.28 ± 0.11 mM; *p*-value 0.3). The kcat was 8.9 ± 3.4 nmol/min for hGC-C and 0.34 ± 0.1 nmol/min for mGC-C, demonstrating the compromised catalytic activity of mGC-C.

We then asked whether the reduced catalytic activity was a property solely of the GCDs of the two receptors. We created chimeric constructs where the GCDs were swapped (Figs. 3*D* and S2). Alignment of the sequences of human and rodent GC-C shows the deletion of one amino acid near the linker region of mGC-C (Fig. S3), which explains the altered residue numbers shown for constructs containing the cyclase domain of mGC-C. The chimeric receptors were expressed and binding to ST, as expected, was determined by the ECD (Fig. 3*E*). Cells were stimulated with ST and cGMP production monitored. The chimeric receptor where the mouse GCD was exchanged with that in the human receptor (hmCYC) showed a log order reduction in cGMP accumulation when compared to hGC-C but was but was ∼ 10-fold higher than mGC-C. Further, cGMP production by the chimera where the mouse GCD was exchanged with that of the human receptor (mhCYC) showed an increase in cGMP levels in comparison with the mGC-C (∼8-fold; Fig. 3*F*), though still lower than that of hGC-C. Swapping of the human cyclase domain with the mouse catalytic domain revealed a significant reduction in Vmax of hGC-C (hGC-C, 8.4 ± 1.5 nmol/pmol receptor; hmCYC, 1.6 ± 0.1 nmol/pmol receptor; *p* value 0.01). Further, replacement of the human GCD in mGC-C resulted in an increase in Vmax of mGC-C (mGC-C, 0.4 ± 0.1 nmol/pmol receptor; mhCYC 1.7 ± 0.2 nmol/pmol receptor; *p* value 0.004; Fig. 3*G*). These results reveal that the GC activity of GC-C is not solely determined by the catalytic domain but is also modulated by the associated KHD and ECD.

Allosteric regulation by ATP

The pseudokinase domain in receptor GCs acts as an allosteric regulator of catalytic activity, and by binding ATP, modulates ligand-mediated activation (19). Nonionic detergents activate receptor GCs by unknown mechanisms but could involve interactions between the linker region and catalytic domain (20). ATP inhibits Lubrol-stimulated GC activity in the presence of Mg^{2+} as the metal ion cofactor and the inhibition is lost in a mutant form of GC-C, where the lysine residue critical for ATP binding is mutated to an alanine (GC-C_{K516A}; (25)). However, ATP inhibits GC activity when Mn^{2+} is the metal ion used in assays. This inhibition is also seen in the GC-C_{K516A} mutant receptor, indicating that a second allosteric site that binds MnATP lies in the GCD of hGC-C (25).

GC activity of mGC-C in the presence of MgGTP was lower than that of hGC-C (Fig. 4*A*). We monitored Lubrol-mediated stimulation of hGC-C, mGC-C, and chimeras in the presence of MgGTP and observed that the ATP-mediated inhibition was lost in mGC-C and mhCYC chimera (Fig. 4*A*), but retained in the hmCYC chimera, indicating that the

concentrations of ST. Experiments were performed at least thrice and the mean ± SD of the IC_{50} calculated are shown. The *p* value is < 0.001. *F*, binding of ^{125}I-labeled ST_{Y72F} peptide in the presence of varying concentrations of mouse uroguanylin for mouse GC-C and human uroguanylin for human GC-C (homologous, *left*) or mouse uroguanylin for human GC-C and human uroguanylin for mouse GC-C (heterologous, *right*). Sequence alignment of mature human and mouse uroguanylin displaying changes in amino acids is shown on the top. Inset values represent the mean IC_{50} ± SD of determinations of experiments repeated three times. The *p* values for datasets are < 0.001. *G*, binding of ^{125}I-labeled ST_{Y72} peptide to monolayers of HEK293E cells expressing either human or mouse GC-C (*top*). Each *dot* represents an independent experiment with two experimental duplicates in each experiment. *Bottom panel* shows the percentage of GC-C trafficked to the plasma membrane out of total GC-C expressed in the cell. Data shown is analyzed across four experiments. *H*, schematic displaying the domains of the human and mouse chimeric GC-C receptor (*left*). Western blot analysis of membrane protein prepared from HEK293E cells expressing either WT or chimeric GC-C receptor, showing that the ECD determines differential mobility on SDS-PAGE (*top panel*). Binding of ^{125}I-labeled ST_{Y72F} peptide in the presence of varying concentrations of ST (*bottom panel*). Inset table represents the mean IC_{50} ± SD from individual experiments repeated thrice. Comparisons between *p* values were made using ordinary one-way ANOVA and are hGC-C *versus* mGC-C, <0.001; hGC-C *versus* hmICD, 0.99; mGC-C *versus* mhICD, 0.59; hGC-C *versus* mhICD, < 0.001; mGC-C *versus* hmICD, < 0.001. GC-C, guanylyl cyclase-C; ST, stable enterotoxin.

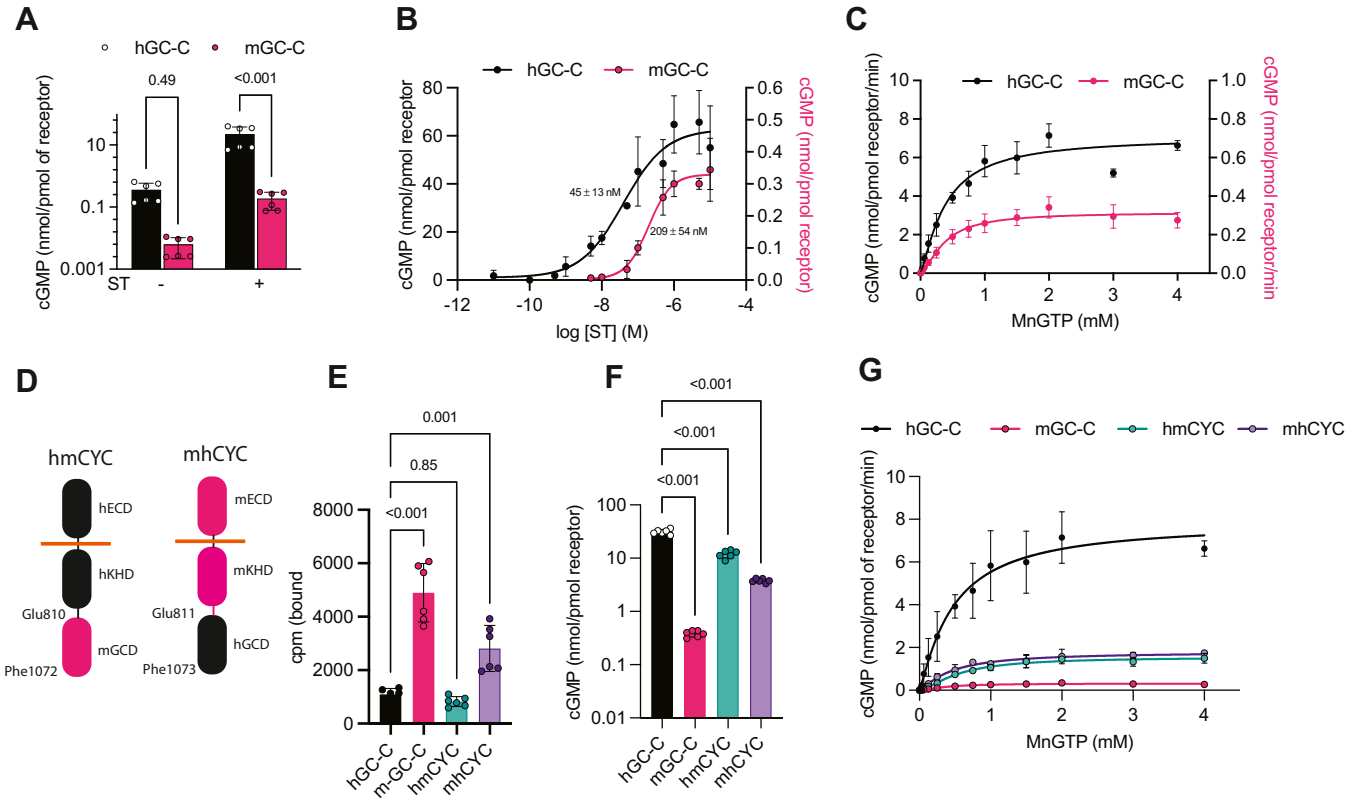

Figure 3. Catalytic activities of mGC-C and hGC-C. *A*, HEK293E cells expressing either human or mouse GC-C were treated with medium alone, or 10^{-6} M ST and cGMP produced estimated by radioimmunoassay. Values shown are the mean ± SD from three independent experiments with experimental triplicates in each experiment. *p* values were determined using two-way ANOVA. *B*, HEK293E cells expressing either human or mouse GC-C were treated with the indicated concentrations of ST and cGMP measured by radioimmunoassay. Cyclic GMP produced was normalized to receptor concentrations (see Experimental procedures). Cyclic GMP produced by human GC-C is shown on the *left y*-axis and mouse GC-C on the *right y*-axis in log scales. Values represent mean ± SD from experiments performed thrice. Inset values represent the mean EC_{50} ± SD of determinations of experiments repeated thrice. *C*, *in vitro* GC assays performed on membranes prepared from HEK293E cells expressing either human or mouse GC-C in the presence of varying concentrations of MnGTP as substrate. cGMP produced by human GC-C is shown on *left y*-axis and mouse GC-C on *right y*-axis, respectively. Values represent mean ± SD from experiments performed thrice. *D*, schematic cartoon displaying the domains of the human and mouse guanylyl cyclase domain (GCD) chimeric GC-C receptors. *E*, binding of ^{125}I-labeled ST_{Y72} peptide on the monolayers of HEK293E cells expressing either WT or GCD chimeric GC-C. Values represent mean ± SD. Each *dot* represents an independent experiment with two experimental duplicate each time. *p* values were obtained using ordinary one-way ANOVA. *F*, HEK293E cells expressing either WT or GCD chimeric GC-C were treated with 10^{-6} M ST and cGMP measured by radioimmunoassay. Cyclic GMP produced was normalized to receptor concentrations. Values represent mean ± SD. Each *dot* represents an independent experiment with two experimental duplicate each time. *p* values were obtained using one-way ANOVA with Welch's correction. *G*, *in vitro* guanylyl cyclase assay for membrane prepared from HEK293E cells expressing either WT or GCD chimeric GC-C in the presence of varying concentrations of MnGTP as substrate. Values represent mean ± SD from experiments performed thrice. GC-C, guanylyl cyclase-C; ST, stable enterotoxin.

pseudokinase domains of the mouse and human receptor varied in terms of their allosteric regulation of their associated catalytic domains. However, ATP-mediated inhibition of GC activity in the presence of MnGTP remained (Fig. 4*B*), suggesting that the allosteric MnATP-binding site was present in the catalytic domains of both mGC-C and hGC-C.

Differential effects of pharmacological regulators of hGC-C

Linaclotide and plecanatide are peptide therapeutics used for the treatment of constipation and chronic visceral pain (17, 26). In initial preclinical models, linaclotide was administered intravenously or by gavage at concentrations of 8 mg/kg body weight (27), while dosages in humans is recommended at ∼ 200 μg once daily (28). The exceptionally high doses used in rodents can be explained by the lower affinity of linaclotide to mGC-C than for hGC-C (IC_{50} for hGC-C 8.7 ± 0.7 nM; mGC-C 35 ± 3 nM; *p* value 0.004; Fig. 5*A*). This naturally implies that certain peptide/small molecule analogs that are directed to the ECD of GC-C may be poorly active in preclinical models but nevertheless show efficacy in humans or cell lines derived from human tissue.

N-2-(propylamino)-6-phenylpyrimidin-4-one substituted piperidines were found to inhibit cGMP accumulation in response to the ST peptides. Of these, SSP2518 was found to be specific to GC-C and did not inhibit cAMP-mediated chloride secretion by cystic fibrosis transmembrane conductance regulator (16). Interestingly, these inhibitors did not inhibit ST-mediated anion secretion in the mouse intestine, but were efficacious in the pig and human intestine, prompting the authors to suggest that these inhibitors did not bind to the cyclase domain, given the high degree of conservation of the GCD across these proteins (16). We, therefore, asked if the chimeras we had generated in this study could be used to identify the binding site of SSP2518. We treated cells expressing either hGC-C, mGC-C, or the chimeric constructs with SSP2518 and measured ST-mediated cGMP production.

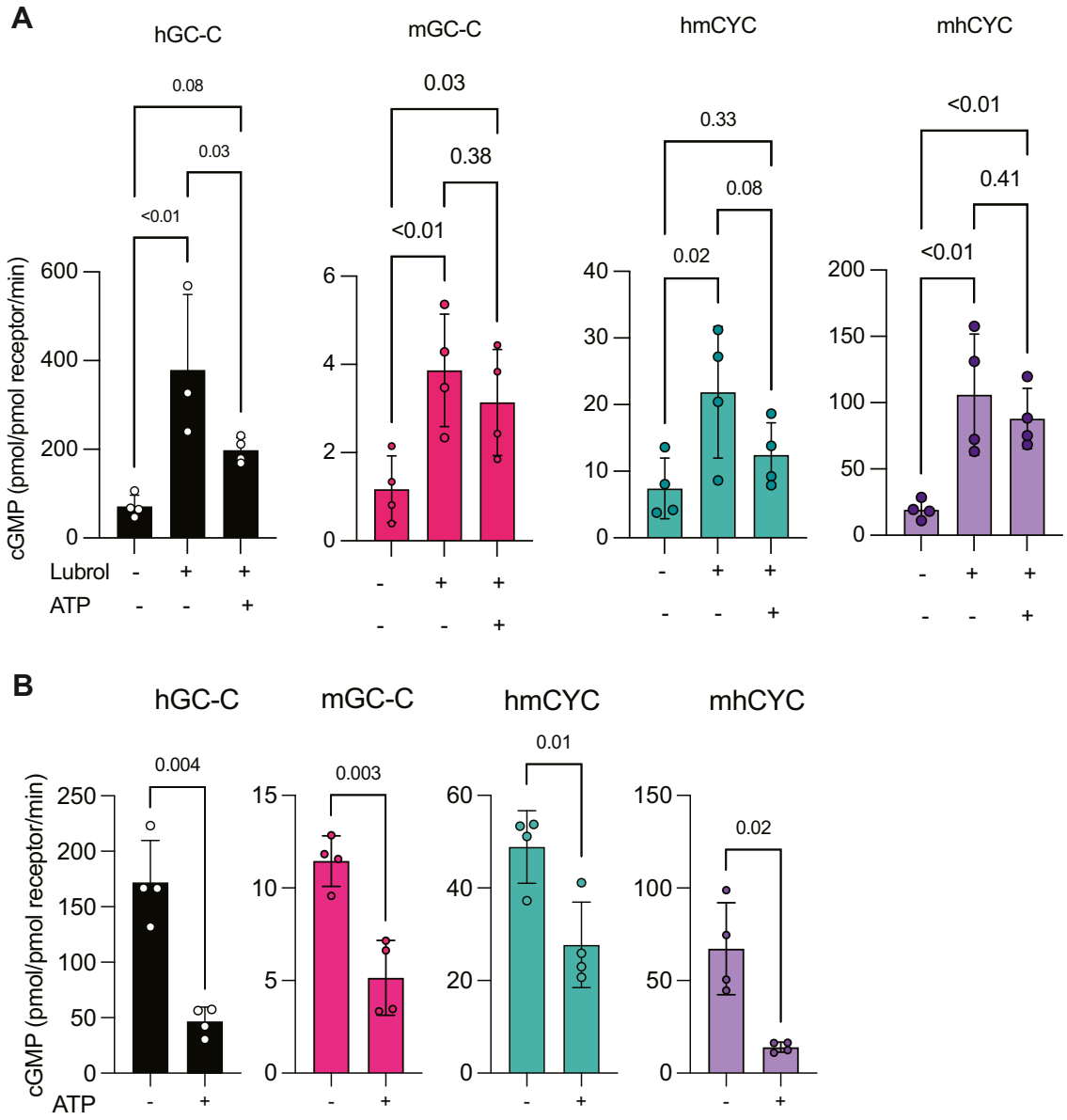

Figure 4. Mouse GC-C displays no allosteric inhibition of guanylyl cyclase activity in the presence of ATP. *A*, *in vitro* guanylyl cyclase assay using the membrane prepared from HEK293E cells expressing either WT or GCD chimeric GC-C receptors with MgGTP as substrate in the presence of Lubrol or Lubrol + ATP. Values represent mean ± SD. Each *dot* represents an independent experiment with two experimental duplicates each time. *p* values were obtained using ordinary one-way ANOVA. *B*, *in vitro* guanylyl cyclase assay using the membrane prepared from HEK293E cells expressing either WT or GCD chimeric GC-C receptors with MnGTP as substrate in the presence or absence of ATP. Values represent mean ± SD. Each *dot* represents an independent experiment with two experimental duplicates each time. *p* values were obtained using an unpaired, two-tailed *t* test. GC, GC, guanylyl cyclase; GCD, guanylyl cyclase domain; ST, stable enterotoxin.

While SSP2518 treatment did not alter the expression of the hGC-C, mGC-C, or the chimeric receptors (Fig. 5*B*, upper panel), cGMP production was inhibited in the presence of the inhibitor in constructs that contained either the intracellular domain from hGC-C or only the human cyclase domain (Fig. 5*B*). Neither mGC-C or the chimeric constructs containing the mouse intracellular domain or the GCD from mGC-C showed a reduction in cGMP production (Fig. 5*B*).

What was striking was the almost complete inhibition of the mhCYC chimera (Fig. 5*B*). We therefore monitored the IC_{50} of SSP2518 in GC assays performed with hGC-C and chimeras containing the human GCD and observed a significantly lower IC_{50} for mhCYC than either hGC-C or mhICD (Fig. 5*C*). These results show that SSP2518 binds to the GCD of hGC-C but the presence of the mouse ECD and KHD domains can subtly modify binding affinity. Further, this again emphasizes the fact that molecules which are ineffective in rodent models may interact and modify the activity of hGC-C.

Discussion

Mice models are useful in studying human biology and disease due to the phylogenetic relationship, genetic, and physiological similarities of mice to humans. The ease of

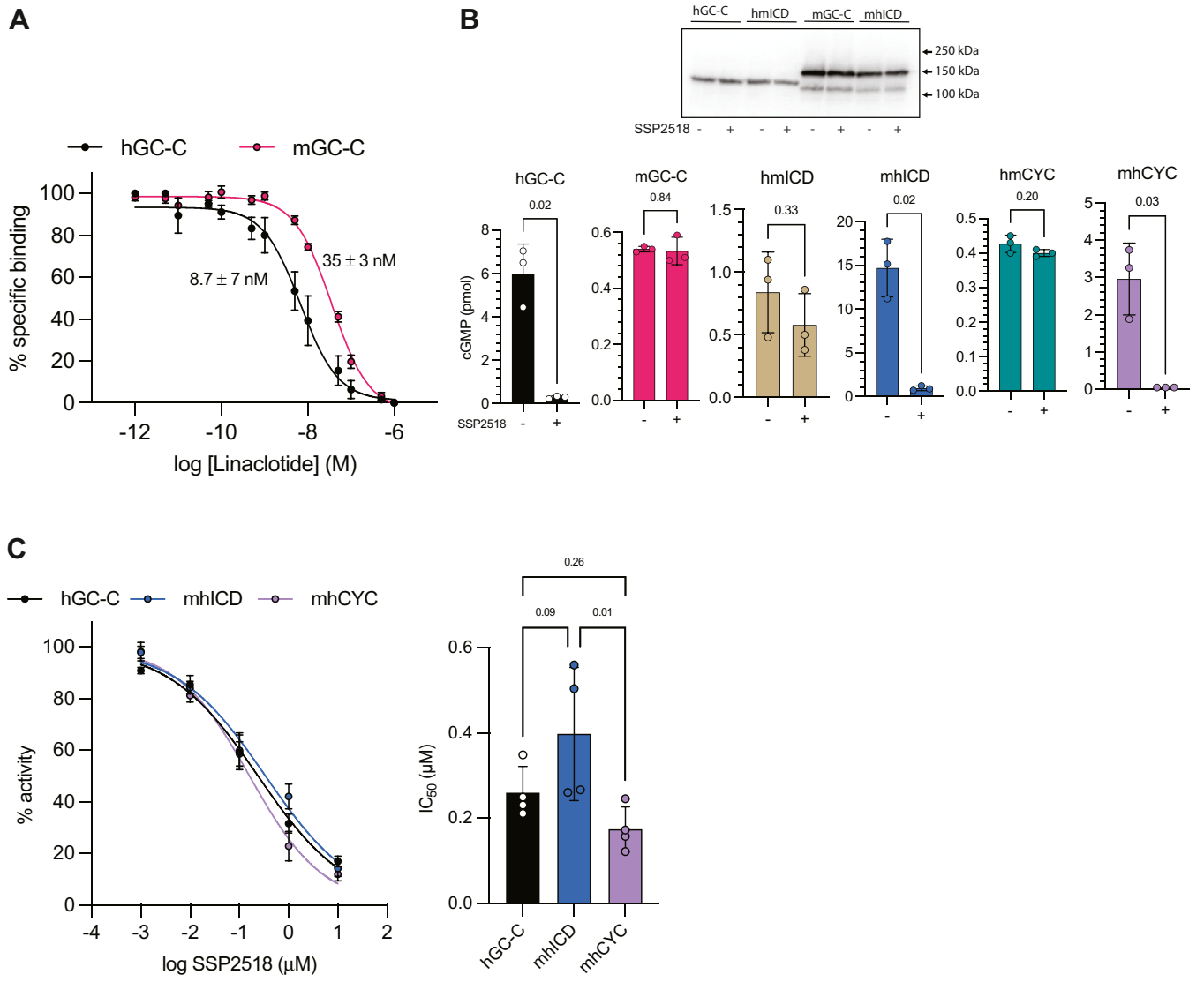

Figure 5. Human GC-C pharmacological inhibitor fails to inhibit mouse GC-C activity. *A*, binding of ^{125}I-labeled ST_{Y72F} peptide in the presence of varying concentrations of linaclotide. Experiments were performed at least thrice and the mean ± SD of the IC_{50} calculated are shown. The *p* value is < 0.004. *B*, inhibition of cGMP production by SSP2518. Cells transfected with the indicated receptors were treated with 10 μM SSP2518 or 1% dimethlysulfoxide for 30 min, followed by the addition of ST (10^{-6} M). Expression of the receptors was checked in the absence or presence of SSP2518 by Western blotting (*top panel*) and cGMP produced was measured (*bottom panel*). Values represent mean ± SD. Each *dot* represents an independent experiment with two experimental duplicates. *p* values were obtained using an unpaired, two tailed *t* test. *C*, *in vitro* guanylyl cyclase assay using the membrane prepared from HEK293E cells expressing either WT or chimeric GC-C receptors with MnGTP as substrate in the presence of varying concentration of inhibitor in 1% dimethlysulfoxide (*left*). Data shown is the mean ± SD obtained from three independent experiments. *Right panel* shows the IC_{50} ± SD for human GC-C, and chimeric GC-C harboring either human GCD or human intracellular domain (ICD). Values represent mean ± SD. *p* values were obtained using ordinary one-way ANOVA. C; cGMP, 3′,5′-cyclic GMP; GC-C, guanylyl cyclase-ST, stable enterotoxin.

maintenance and breeding, availability of inbred strains and tools to create knock out, knock in, and transgenic strains of mice has added much strength to mouse research (29). However, some mouse models of genetic diseases fail to produce the same phenotype seen in human patients or respond differently to interventions than humans (12, 29). For example, mutations in Bruton's tyrosine kinase, which is important for B cell development, cause complete ablation of B cell development in humans, whereas a mouse disease model displays a less severe phenotype (30). Similarly, endostatin, which killed cancer cells in the mouse, has no effect on human cancers (29).

Mouse models have been used to understand the role of GC-C for the past 4 decades (6, 12, 13). Mouse and hGC-Cs share 85% amino acid sequence identity (Fig. S3). Functional conservation of GC-C signaling is evident between mice and humans as ST treatment in mice leads to the accumulation of fluid in the gut (31, 32). Further, a mutation corresponding to that which causes FGDS in humans resulted in a hyperactive GC-C with phenotypes seen in mice resembling those seen in patients (6). Inactivating mutations in GC-C in humans result in loss of fluid-ion homeostasis, meconium ileus, and constipation (15, 33). However, mice lacking GC-C show no compromise in fluid-ion homeostasis in the intestine (12). Hyperactive mutations in GC-C leads to a fully penetrant syndrome of diarrhea in humans (34, 35), while inactivating mutations of GC-C do not display 100% penetrance (15, 33),

indicating compensatory pathways in maintaining fluid-ion homeostasis in the gut during reduced GC-C signaling in humans and the mouse.

Our results show that mGC-C is compromised in its binding and catalytic activity compared to hGC-C (Figs. 2 and 3) that account for the high dose of linaclotide used in preclinical studies using rodent models (100 μg to 8 mg/kg body weight) (4). The US Food and Drug Administration-approved dose for human is approximately 5 μg/kg body weight (11). We now show that this can be attributed to the log order lower affinity of mGC-C for ST peptide and linaclotide (Figs. 2 and 5). FGDS patients with p.S840I mutation displayed early onset of diarrhea ranging from 3 to 20 stool per day (34), whereas the mouse model with corresponding mutation displayed intestinal anomalies similar to FGDS, but no signs of watery diarrhoea (6). The lower GC activity of GC-C in the mouse gut may reduce the extent of fluid secretion into the lumen and therefore hydration of stool.

A sequence of amino acids (SPTFIWK) in the ECD of the porcine receptor is identical to that seen in hGC-C and was shown to be important for ligand binding (Fig. S3) (36). The sequence in mGC-C is NPNFIWK and may affect the binding affinity for ligands. Mouse GC-C traffics better to the cell surface in HEK cells, and if this is true in intestinal epithelial cells, the higher concentration of GC-C on the cell surface may compensate for its lower activity in terms of cGMP production, since a larger amount of GC-C is available for ligand stimulation.

The functional and structural similarities between human and mGC-C, despite the biochemical differences are evident from the fact that the chimeric receptors used in this study were active, ligand-stimulated GCs. This conservation of domain–domain interactions between mouse and hGC-C is interesting, since this is not observed between different human receptor GCs where replacing the KHD of GC-A with the KHD of GC-C led to the inactivation of GC-A (37). The GC activity of chimeras differed from native GC-Cs, suggesting that cGMP production may not only be dependent on the GCD alone but an interplay with domains N terminal to the GCD that undergo structural and conformational changes to bring about cGMP production upon ligand binding to ECD of GC-C.

ATP is known to inhibit *in vitro* MnGTP-mediated and detergent-mediated GC activity by binding to the cyclase domain or KHD, respectively (38). Interestingly, mGC-C and the chimeric receptor harboring the mouse KHD showed no inhibition of detergent-mediated activity by ATP. This property was seen following mutagenesis of the linker region of GC-C, suggesting that detergents disrupt the interactions between the linker and the GCD/KHD (38). These interactions between the linker and the GCD of mGC-C may diverge from those in hGC-C. Recent, high-resolution cryo-EM structures of soluble guanylyl cyclase revealed dramatic conformational changes that take place upon enzyme activation by binding of NO to the heme moiety present in the N terminus of the protein (39). In the unliganded, unactivated state, soluble guanylyl cyclase adopts a contracted conformation because of bending of coiled-coil regions resembling the linker region in receptor GCs. Upon activation, the regulatory lobe rotates relative to the catalytic domain, the protein elongates, and the portion of the linker region bent in the inactive state straightens to form long extended helices, allowing rearrangements in the GCD that allow catalysis (39). If a similar rotation is required in GC-C to allow catalytic domain activation, then detergents may allow changes in the conformation of the linker region in hGC-C but may occur to a less extent in mGC-C. However, mGC-C and hmCYC displayed ATP-mediated inhibition of MnGTP-mediated activity (Fig. 4, *A* and *B*), indicating that the overall structure of the GCD, including the ATP-binding, allosteric site, is conserved in both receptors.

GC-C is a multidomain protein. AlphaFold 2 generates structures of the kinase homology domain and the GCD of GC-C with high confidence. However, the structure generated by AlphaFold 2 for the entire intracellular domain shows very poor confidence in the linker region and the juxtamembrane domain. As, we have reported in this study, it is not the properties of the GCD alone that determine the enzymatic potential of GC-C, but interdomain interactions might be different between human and mGC-C. In fact, there is no appreciable difference in the structure of mouse and hGC-C as predicted by AlphaFold 2, though we clearly see dramatic differences in their activity. Therefore, AlphaFold models do not provide us with a reliable tool to understand GC-C structure and the associated properties.

Recently, a cryo-EM structure of hGC-C in complex with Hsp90 and Cdc37 was reported (40). The authors engineered the dimerization of the receptor using a leucine-zipper domain to replace the ECD and solved the cryo-EM structure of the KHD in complex with Hsp90 and Cdc37, which naturally copurified with the receptor expressed in CHO cells. The N-terminal region to the KHD (*i.e.*, the juxtamembrane region) was unstructured, as were regions C-terminal to the KHD (*i.e.*, the linker and the GC domains). The association with chaperones suggests that the structure of the KHD was the non-native structure, perhaps undergoing folding with assistance from Hsp90 and Cdc37. Therefore, this cryo-EM structure of KHD of hGC-C did not provide us with information to understand the structural basis of GC-C activation further., since we have shown the critical role of the linker region in mediating GC activity of receptor GCs (38).

Using chimeric constructs of mouse and hGC-C allowed us to delineate the binding site for SSP2518, the only known specific inhibitor of GC-C (Fig. 5*B*) (16). We could demonstrate that the inhibitor binds to the GC domain of hGC-C and not to the mouse catalytic domain (Fig. 5*B*), even though the sequence identity between these two domains is >90% (Fig. S3). Introduction of the KHD of mGC-C upstream of the human GC domain significantly altered the IC_{50}, however, again reiterating that the *in vitro* cyclase activity of GC-C is a result of interdomain interactions (Fig. 5*C*).

In summary, we have studied the biochemical properties of mouse and hGC-C in detail. Our results suggest that it is imperative to evaluate agonists and antagonists that regulate GC-C activity in preclinical models, bearing in mind the significantly different biochemical properties of the two receptors. Appreciating these biochemical differences would lead

to better approaches while using the mouse as a preclinical model to study compounds regulating GC-C activity, mimicking human mutations in GC-C in knock in mice, and deciphering various roles that GC-C might play in the human intestine.

Experimental procedures

Cloning of mouse variants of GC-C

RNA was prepared from mouse colonic tissue and converted to complementary DNA (cDNA) by reverse transcription using random primers. Primers (Table S1) were designed to amplify the 5′ region of the cDNA (mGCC_Fwd_Xho1and mGCC1677r Sca1) and the 3′ region (mGCC1677 Sca1 and mGCCrevXba1) and two PCR products cloned independently into the pGEMT-Easy vector. Inserts were sequenced (Macrogen) and then fragments obtained by Xho1-Sca1 digestion of the 5′ clone and Sca1-Xba1 digestion of the 3′ clone were ligated in the mammalian expression vector pcDNA3 digested with Xho1 and Xba1. Variant 2 of mGCC was obtained as a cDNA clone from Transomic Technologies in the vector pSPORT1 (clone ID BC099968). The clone was sequenced before subcloning into pCDNA3 using suitable restriction enzymes.

Real-time quantitative PCR from mouse intestine

Real-time PCR was performed using SYBR Premix Ex Taq (Tli RNase H Plus) on a CFX96 Touch real-time PCR detection system (Bio-Rad). *Gapdh* was used as internal normalization control. The primer sequences used are shown in Table S1.

Generation of HEK293E cells with stable expression of GC-C using retroviral transduction

Retrovirus-like particles were packaged in HEK293 E cells using pMX plasmid vector, pCMV-Gag-Pol and pCMV-VSV-G (kind gifts from Dr Avinash R. Shenoy, Imperial College London). To perform this, cDNA sequences of GC-Cs was cloned into pMX plasmid vector. HEK293E cells (obtained from The American Type Culture Collection) were transfected with pMX plasmid, pCMV-VSV-G, and pCMV-Gag-Pol in 3:2:1 ratio. The media containing the retrovirus was collected 48 h posttransfection and filtered through a 0.45-μm syringe filter. Virus was concentrated from the filtrate by adding PEG-6000 (Sigma-Aldrich) and NaCl at a final concentration of 8.5% (w/v) and 400 mM, respectively, followed by centrifugation at 7000*g* for 20 min at 4 °C. To perform transduction of HEK293E cells, polybrene was added to the cells at a final concentration of 8 μg/ml, followed by a gentle addition of 100 μl of concentrated retrovirus particles. After 48 h of transduction, the media was replaced with complete media supplemented with 2 μg/ml puromycin for the selection of transduced cells. The media was replaced every third day, and the cell line with stable expression of GC-C was confirmed using radioligand binding assays and Western blot analysis.

Heterologous transient expression of WT and chimeric GC-C receptors in HEK293E cells was achieved by transfecting HEK293E cells with pcDNA3 plasmid containing the cDNA sequence of WT or mutant GC-C using Lipofectamine 2000. Assays were performed 72 h post transfection and expression of GC-C was confirmed using radioligand binding assays and Western blot analysis.

Cloning of GC-C chimeric constructs

Strategies for the cloning of chimeric constructs and amino acid boundaries are shown in Fig. S2. Catalytic domain chimeras were generated at the junction between the linker and the GCD from residues 811 in hGC-C (and 810 in mGC-C). The sequence at the junction includes the residues KSLKEKG, which is identical in both hGC-C and mGC-C. The codon for Leu (CTG) in this sequence was replaced by CTT in suitably designed primers, thereby introducing a silent AflII site (Table S1). Neither hGC-C nor mGC-C coding sequences contain a site for AflII. Primers used for PCR are shown in Table S1 and used to amplify the region of hGC-C upstream of the GCD or the catalytic domain of mGC-C using primers containing AflII sites, T3 or T7 primers using hGC-C and mGC-C cloned into the pBSK vector as templates. PCR products were digested with AflII and cloned into Xho1-Xba1–digested pCDNA3 to generate hmCYC and mhCYC and verified by sequencing.

An overlap extension PCR-based protocol was followed to generate the hmICD and mhICD constructs (Fig. S2) (41). The first PCR generated two products with overlapping sequences at the junction site. These PCR products using primers shown in Table S1 were used for a second PCR to generate a full-length chimeric sequence, cloned into pcDNA3, and verified by sequencing.

Preparation of membrane fraction from HEK293E cells

Confluent cell monolayers were washed with chilled PBS (10 mM sodium phosphate buffer, pH 7.2, and 0.9% sodium chloride) and scraped into homogenization buffer (50 mM Hepes, pH 7.5, 100 mM NaCl, 5 mM EDTA, 1 mM DTT, 5 μg/ml soybean trypsin inhibitor, 5 μg/ml leupeptin, 5 μg/ml aprotinin, 2 mM PMSF, and1mM sodium orthovanadate). The cell lysate was sonicated and centrifuged at 12,000*g* for 60 min at 4 °C. The pellet obtained was resuspended in a buffer containing 50 mM Hepes, pH 7.5, 10 μg/ml leupeptin, 10 μg/ml aprotinin, 1 mM sodium orthovanadate, and 20% glycerol. The protein concentration was estimated by using a modification of the Bradford protein assay (42).

To inhibit N-linked glycosylation, a monolayer of HEK293E cells expressing GC-C were treated with 20 μg/ml of tunicamycin for 24 h, followed by membrane preparations and Western blot analysis. For enzymatic deglycosylation of GC-C post expression in HEK293E cells, membrane protein from cells expressing GC-C was resuspended in 50 mM sodium phosphate buffer, pH 7.2, containing protease inhibitors. PNGase F (1500 units; Sigma) was added, and incubation was continued at 4 °C for 12 h. Treated or untreated membrane protein was then subjected to Western blot analysis using GC-C mAb.

Western blot analysis

Membrane proteins isolated from HEK293E cells were resolved on 7.5% SDS-PAGE and transferred onto polyvinylidene fluoride membrane in transfer buffer (25 mM Tris base, 192 mM glycine, 20% methanol, pH 8.3) using semidry transfer equipment (Trans-Blot Turbo, Bio-Rad) at 25 mV and 1 A for 15 min. The membranes were then rinsed in 10 mM Tris-Cl, pH 7.2, 100 mM NaCl, 0.1% Tween 20 (TBS-T) and blocked for 1 h at room temperature in 2% blocking solution prepared in TBS-T. The membrane was incubated with primary antibody overnight (12–14 h) at 4 °C, followed by three times wash with TBS-T. The membrane was incubated with anti-mouse IgG conjugated to horseradish peroxidase for 1 h at room temperature, followed by washing three times with TBS-T. Immunoreactive bands were visualized by chemiluminescence detected using Immobilon reagent as per manufacturer's instruction on Chemidoc XRS+ (Bio-Rad).

Receptor binding assay

An analog of ST, ST_{Y72F} was iodinated using $Na^{125}I$ and prepared in the laboratory as described in (43). To perform radioligand binding assay on an intact monolayer of cells, confluent monolayers of HEK293E cells, seeded in a 24-well plate expressing GC-C were washed with 1 ml of Dulbecco's modified Eagle medium (DMEM)-HG containing 0.2% BSA. Cells were incubated with 150,000 cpm of ^{125}I-labeled ST_{Y72F} prepared in DMEM-HG containing 0.2% BSA for 1 h at 37 °C. Cells were treated with 5 × 10 to 7 M ST to determine nonspecific bound counts. Cells were washed twice with cold DMEM-HG containing 0.2% BSA and lysed in 0.1 N HCl. The amount of radioligand ST bound was determined using a gamma counter.

For competitive receptor binding assay, crude membrane protein (50 μg) was incubated in binding buffer (50 mM Hepes, pH 7.5, 4 mM $MgCl_2$, 0.1% BSA) with varying concentrations of unlabeled ST (10^{-5} to 10^{-12} M), linaclotide, or uroguanylin-binding buffer (50 mM MES, pH 5.5, 4 mM $MgCl_2$, 0.1% BSA) with varying concentration of uroguanylin (10^{-5} to 10^{-12} M) in the presence of 100,000 cpm of ^{125}I-labeled ST_{Y72F} for 1 h at 37 °C. Following incubation, samples were filtered through GF/C filters and washed with 5 ml of 10 mM sodium phosphate buffer, pH 7.2 containing 0.9% NaCl, and 0.2% BSA through a filtration unit. The associated radioactivity with the filters was estimated by a gamma counter. Competitive binding analysis and determination of IC_{50} values were performed using GraphPad Prism 10 (https://www.graphpad.com) and the Hill coefficient was constrained to −1 in the analysis with the assumption that there is a single binding site per molecule of receptor.

Measurement of ligand-stimulated cGMP production in HEK293E cells

Ligand-stimulated cGMP production in HEK293E expressing GC-C was performed by incubating cells with DMEM-HG containing serum and antibiotics along with 500 μM 3-isobutyl-1-methylxanthine (IBMX) for 30 min at 37 °C in a humidified CO_2 incubator. This was followed by treatment of cells with 10^{-6} M ST for 30 min. The media was removed, and monolayers were lysed in 0.1 N HCl and cGMP produced by cells was estimated using radioimmunoassay (RIA) (43). For ligand dose-response assay, monolayers were incubated in DMEM-HG containing serum and antibiotics along with 500 μM IBMX for 30 min, followed by treatment with varying dose of ST (10^{-5} to 10^{-9} M) for 30 min. Cells were lysed and intracellular cGMP produced was estimated using RIA, as described earlier (43).

For assays performed with SSP2518, the compound was dissolved in dimethlysulfoxide and added to cells a final concentration of 10 μM and 1% dimethlysulfoxide in a medium containing 500 μM IBMX. Cells were cultured for 30 min at 37 °C in a humidified CO_2 incubator, treated with 10^{-6} M ST for 30 min, and processed for measurement of cGMP production as above.

In vitro *GC assays*

Crude membrane prepared from HEK293E cells expressing GC-C were used for *in vitro* GC assay with MnGTP or MgGTP as substrate. *In vitro* GC activity with MnGTP as substrate was measured using 10 μg of membrane incubated in the assay buffer (60 mM Tris-Cl, pH 7.5, containing 500 μM IBMX, and an NTP-regenerating system consisting of 7.5 mM creatine phosphate, and 10 μg/ml creatine phosphokinase) in the presence of fixed (1 mM) or varying concentrations (20 μM to 4 mM) of MnGTP, with free metal concentrations maintained at 4 mM.

In vitro GC activity with MgGTP as substrate was measured by incubating membrane protein (10 μg) with assay buffer with 1 mM MgGTP as substrate with 4 mM free $MgCl_2$ at 4 °C, following which the reaction mixture was incubated at 37 °C for 10 min. Detergent-mediated activity was measured by incubating membrane protein with assay buffer containing 0.1% of Lubrol-PX using 1 mM MgGTP as substrate and 4 mM of free $MgCl_2$. All the reaction mixtures were incubated at 37 °C for 10 min.

To analyze ATP-mediated responses, the reaction was carried out in the presence of 1 mM MgATP/MnATP with 1 mM MgGTP/MnGTP as substrate and 4 mM of free metal ion in presence or absence of 0.1% of Lubrol-PX. To analyze inhibition by SSP2518 *in vitro*, the reaction was carried out in the presence of 1 mM MnGTP as substrate and 4 mM of free metal ion in the presence or absence of the indicated concentrations of SSP2518. The concentrations of free Mg^{2+} or Mn^{2+} and MnGTP/MgGTP/MnATP/MgATP complexes present in assays were calculated using Maxchelator version 2.51 (http://www.stanford.edu~cpatton/maxc.html). GC assays were terminated by the addition of ice-cold 50 mM sodium acetate buffer, pH 4.75, followed by boiling of the samples at 95 °C for 5 min. The reaction mixture was centrifuged, and the amounts of cGMP present in the supernatant was estimated using RIA.

cGMP produced by cells or during *in vitro* GC assay was normalized to the receptor amounts present on the cell's surface or in the membrane preparations, respectively as

described earlier (6). Briefly, total receptor amounts or Bmax was determined on the surface of cells or in membrane preparations using ^{125}I-labeled ST_{Y72F} peptide, using the equations below.

$$Bmax = \frac{[Specific\ bound]}{Fractional\ Occupancy} = \frac{[Specific\ bound]}{[radioligand]/(Ki+[radioligand])}$$

where Bmax is the total number of receptors expressed; [specific bound] is the concentration of specific bound ^{125}I-labeled ST_{Y72F}; [radioligand] is the concentration of ^{125}I-labeled ST_{Y72F} used in the assay, and Ki is the apparent dissociation equilibrium constant, which is obtained from the IC_{50} data. For ST peptide, this is taken as 6.7 nM for mGC-C and 0.65 nM for hGC-C.

Data analysis

Data was analyzed using GraphPad Prism 9. Details of statistical analysis used are provided in the legends to the Figures.

Data availability

All data are contained within the manuscript.

Supporting information—This article contains supporting information.

Acknowledgments—This paper is dedicated to the memory of Prof. Hugo De Jonge, Erasmus University, Rotterdam, Netherlands. We would like to thank Dr Marcel Bijvelds of Erasmus University for providing SP2158. We acknowledge the technical assistance of Saurabh Kumar and Tejeswani Padma in this work.

Author contributions—V. M. and S. S. V. conceptualization; V. M., K. S., and A. B. data curation; V. M., K. S., A. B., P. M., and S. S. V. formal analysis; S. S. V. funding acquisition; V. M., K. S., and A. B. investigation; V. M., K. S., and A. B. methodology; S. S. V. project administration; S. S. V. supervision; V. M. and S. S. V. writing-original draft; V. M., K. S., A. B., P. M., and S. S. V. writing-review and editing.

Funding and additional information—K. S. receives a Senior Research Fellowship from the Council of Scientific and Industrial Research. This work was supported by funds from the DBT-Wellcome Trust India Alliance (IA/M/16/1/502606 and IA/TSG/21/1/60025SSV). S. S. V. is a JC Bose National Fellow (SB/S2/JCB-18/2013), and a Margdarshi Fellow supported by the Wellcome Trust DBT India Alliance (IA/M/16/1/502606). Support as National Science Chair by SERB, Government of India (NSC/2022/000019), is also acknowledged.

Conflict of interest—The authors declare that they have no conflicts of interest with the contents of this article.

Abbreviations—The abbreviations used are: cDNA, complementary DNA; cGMP, 3′,5′-cyclic GMP; DMEM, Dulbecco's modified Eagle's medium; ECD, extracellular domain; FGDS, Familial *GUCY2C* diarrhea syndrome; GC, guanylyl cyclase; GCD, guanylyl cyclase domain; hGC-C, human GC-C; IBMX, 3-isobutyl-1-methylxanthine; KHD, kinase homology domain; mGC-C, mouse GC-C; RIA, radioimmunoassay; ST, stable enterotoxin.

References

1. Prasad, H., Shenoy, A. R., and Visweswariah, S. S. (2020) Cyclic nucleotides, gut physiology and inflammation. *FEBS J.* **287**, 1970–1981
2. Mokomane, M., Kasvosve, I., de Melo, E., Pernica, J. M., and Goldfarb, D. M. (2018) The global problem of childhood diarrhoeal diseases: emerging strategies in prevention and management. *Ther. Adv. Infect. Dis.* **5**, 29–43
3. Yim, S. K., Kim, S. W., and Lee, S. T. (2021) Efficient stool collection methods for evaluating the diarrhea score in mouse diarrhea models. *In Vivo* **35**, 2115–2125
4. Busby, R. W., Bryant, A. P., Bartolini, W. P., Cordero, E. A., Hannig, G., Kessler, M. M., *et al.* (2010) Linaclotide, through activation of guanylate cyclase C, acts locally in the gastrointestinal tract to elicit enhanced intestinal secretion and transit. *Eur. J. Pharmacol.* **649**, 328–335
5. Savkovic, S. D., Villanueva, J., Turner, J. R., Matkowskyj, K. A., and Hecht, G. (2005) Mouse model of enteropathogenic Escherichia coli infection. *Infect. Immun.* **73**, 1161–1170
6. Mishra, V., Bose, A., Kiran, S., Banerjee, S., Shah, I. A., Chaukimath, P., *et al.* (2021) Gut-associated cGMP mediates colitis and dysbiosis in a mouse model of an activating mutation in GUCY2C. *J. Exp. Med.* **218**, e20210479
7. Prasad, H., Mathew, J. K. K., and Visweswariah, S. S. (2022) Receptor guanylyl cyclase C and cyclic GMP in health and disease: perspectives and therapeutic opportunities. *Front. Endocrinol. (Lausanne)* **13**, 911459
8. Basu, N., Arshad, N., and Visweswariah, S. S. (2010) Receptor guanylyl cyclase C (GC-C): regulation and signal transduction. *Mol. Cell Biochem.* **334**, 67–80
9. Bose, A., Banerjee, S., and Visweswariah, S. S. (2020) Mutational landscape of receptor guanylyl cyclase C: functional analysis and disease-related mutations. *IUBMB Life* **72**, 1145–1159
10. Chang, W. L., Masih, S., Thadi, A., Patwa, V., Joshi, A., Cooper, H. S., *et al.* (2017) Plecanatide-mediated activation of guanylate cyclase-C suppresses inflammation-induced colorectal carcinogenesis in Apc(+/Min-FCCC) mice. *World J. Gastrointest. Pharmacol. Ther.* **8**, 47–59
11. Love, B. L., Johnson, A., and Smith, L. S. (2014) Linaclotide: a novel agent for chronic constipation and irritable bowel syndrome. *Am. J. Health Syst. Pharm.* **71**, 1081–1091
12. Schulz, S., Lopez, M. J., Kuhn, M., and Garbers, D. L. (1997) Disruption of the guanylyl cyclase-C gene leads to a paradoxical phenotype of viable but heat-stable enterotoxin-resistant mice. *J. Clin. Invest* **100**, 1590–1595
13. Majumdar, S., Mishra, V., Nandi, S., Abdullah, M., Barman, A., Raghavan, A., *et al.* (2018) Absence of receptor guanylyl cyclase C enhances ileal damage and reduces cytokine and antimicrobial peptide production during oral Salmonella enterica serovar typhimurium infection. *Infect. Immun.* **86**, e00799-17
14. Basu, N., Saha, S., Khan, I., Ramachandra, S. G., and Visweswariah, S. S. (2014) Intestinal cell proliferation and senescence are regulated by receptor guanylyl cyclase C and p21. *J. Biol. Chem.* **289**, 581–593
15. Smith, A., Bulman, D. E., Goldsmith, C., Bareke, E., Consortium, F. C., Majewski, J., *et al.* (2015) Meconium ileus in a Lebanese family secondary to mutations in the GUCY2C gene. *Eur. J. Hum. Genet.* **23**, 990–992
16. Bijvelds, M. J., Loos, M., Bronsveld, I., Hellemans, A., Bongartz, J. P., Ver Donck, L., *et al.* (2015) Inhibition of heat-stable toxin-induced intestinal salt and water secretion by a novel class of guanylyl cyclase C inhibitors. *J. Infect. Dis.* **212**, 1806–1815
17. Busby, R. W., Kessler, M. M., Bartolini, W. P., Bryant, A. P., Hannig, G., Higgins, C. S., *et al.* (2013) Pharmacologic properties, metabolism, and disposition of linaclotide, a novel therapeutic peptide approved for the treatment of irritable bowel syndrome with constipation and chronic idiopathic constipation. *J. Pharmacol. Exp. Ther.* **344**, 196–206
18. Team, M. G. C. P., Temple, G., Gerhard, D. S., Rasooly, R., Feingold, E. A., Good, P. J., *et al.* (2009) The completion of the mammalian gene collection (MGC). *Genome Res.* **19**, 2324–2333

19. Mishra, V., Goel, R., and Visweswariah, S. S. (2018) The regulatory role of the kinase-homology domain in receptor guanylyl cyclases: nothing 'pseudo' about it. *Biochem. Soc. Trans.* **46**, 1729–1742
20. Bose, A., and Visweswariah, S. S. (2022) The pseudokinase domain in receptor guanylyl cyclases. *Methods Enzymol.* **667**, 535–574
21. Arshad, N., Ballal, S., and Visweswariah, S. S. (2013) Site-specific N-linked glycosylation of receptor guanylyl cyclase C regulates ligand binding, ligand-mediated activation and interaction with vesicular integral membrane protein 36, VIP36. *J. Biol. Chem.* **288**, 3907–3917
22. Ghanekar, Y., Chandrashaker, A., and Visweswariah, S. S. (2003) Cellular refractoriness to the heat-stable enterotoxin peptide is associated with alterations in levels of the differentially glycosylated forms of guanylyl cyclase C. *Eur. J. Biochem.* **270**, 3848–3857
23. Tiwari, P., Kaila, P., and Guptasarma, P. (2019) Understanding anomalous mobility of proteins on SDS-PAGE with special reference to the highly acidic extracellular domains of human E- and N-cadherins. *Electrophoresis* **40**, 1273–1281
24. Rath, A., Glibowicka, M., Nadeau, V. G., Chen, G., and Deber, C. M. (2009) Detergent binding explains anomalous SDS-PAGE migration of membrane proteins. *Proc. Natl. Acad. Sci. U. S. A.* **106**, 1760–1765
25. Jaleel, M., Saha, S., Shenoy, A. R., and Visweswariah, S. S. (2006) The kinase homology domain of receptor guanylyl cyclase C: ATP binding and identification of an adenine nucleotide sensitive site. *Biochemistry* **45**, 1888–1898
26. Brierley, S. M., Grundy, L., Castro, J., Harrington, A. M., Hannig, G., and Camilleri, M. (2022) Guanylate cyclase-C agonists as peripherally acting treatments of chronic visceral pain. *Trends Pharmacol. Sci.* **43**, 110–122
27. Bryant, A. P., Busby, R. W., Bartolini, W. P., Cordero, E. A., Hannig, G., Kessler, M. M., *et al.* (2010) Linaclotide is a potent and selective guanylate cyclase C agonist that elicits pharmacological effects locally in the gastrointestinal tract. *Life Sci.* **86**, 760–765
28. McWilliams, V., Whiteside, G., and McKeage, K. (2012) Linaclotide: first global approval. *Drugs* **72**, 2167–2175
29. Perlman, R. L. (2016) Mouse models of human disease: an evolutionary perspective. *Evol. Med. Public Health* **2016**, 170–176
30. Conley, M. E., Rohrer, J., Rapalus, L., Boylin, E. C., and Minegishi, Y. (2000) Defects in early B-cell development: comparing the consequences of abnormalities in pre-BCR signaling in the human and the mouse. *Immunol. Rev.* **178**, 75–90
31. Giannella, R. A. (1976) Suckling mouse model for detection of heat-stable Escherichia coli enterotoxin: characteristics of the model. *Infect. Immun.* **14**, 95–99
32. Bolick, D. T., Medeiros, P., Ledwaba, S. E., Lima, A. A. M., Nataro, J. P., Barry, E. M., *et al.* (2018) Critical role of Zinc in a new murine model of enterotoxigenic Escherichia coli diarrhea. *Infect. Immun.* **86**, e00183-18
33. Romi, H., Cohen, I., Landau, D., Alkrinawi, S., Yerushalmi, B., Hershkovitz, R., *et al.* (2012) Meconium ileus caused by mutations in GUCY2C, encoding the CFTR-activating guanylate cyclase 2C. *Am. J. Hum. Genet.* **90**, 893–899
34. Fiskerstrand, T., Arshad, N., Haukanes, B. I., Tronstad, R. R., Pham, K. D., Johansson, S., *et al.* (2012) Familial diarrhea syndrome caused by an activating GUCY2C mutation. *N. Engl. J. Med.* **366**, 1586–1595
35. Muller, T., Rasool, I., Heinz-Erian, P., Mildenberger, E., Hulstrunk, C., Muller, A., *et al.* (2016) Congenital secretory diarrhoea caused by activating germline mutations in GUCY2C. *Gut* **65**, 1306–1313
36. Hasegawa, M., Hidaka, Y., Matsumoto, Y., Sanni, T., and Shimonishi, Y. (1999) Determination of the binding site on the extracellular domain of guanylyl cyclase C to heat-stable enterotoxin. *J. Biol. Chem.* **274**, 31713–31718
37. Koller, K. J., de Sauvage, F. J., Lowe, D. G., and Goeddel, D. V. (1992) Conservation of the kinaselike regulatory domain is essential for activation of the natriuretic peptide receptor guanylyl cyclases. *Mol. Cell Biol.* **12**, 2581–2590
38. Saha, S., Biswas, K. H., Kondapalli, C., Isloor, N., and Visweswariah, S. S. (2009) The linker region in receptor guanylyl cyclases is a key regulatory module: mutational analysis of guanylyl cyclase C. *J. Biol. Chem.* **284**, 27135–27145
39. Liu, R., Kang, Y., and Chen, L. (2021) Activation mechanism of human soluble guanylate cyclase by stimulators and activators. *Nat. Commun.* **12**, 5492
40. Caveney, N. A., Tsutsumi, N., and Garcia, K. C. (2023) Structural insight into guanylyl cyclase receptor hijacking of the kinase-Hsp90 regulatory mechanism. *Elife* **12**, RP86784
41. Heckman, K. L., and Pease, L. R. (2007) Gene splicing and mutagenesis by PCR-driven overlap extension. *Nat. Protoc.* **2**, 924–932
42. Zor, T., and Selinger, Z. (1996) Linearization of the Bradford protein assay increases its sensitivity: theoretical and experimental studies. *Anal. Biochem.* **236**, 302–308
43. Visweswariah, S. S., Ramachandran, V., Ramamohan, S., Das, G., and Ramachandran, J. (1994) Characterization and partial purification of the human receptor for the heat-stable enterotoxin. *Eur. J. Biochem.* **219**, 727–736